SEMARAK ILMU PUBLISHING

Journal of Advanced Research in Numerical Heat Transfer

Journal homepage:
https://semarakilmu.com.my/journals/index.php/arnht/index
ISSN: 2735-0142

Evaluation of Virus Concentration Analysis in the Airway by CFD

Yoshiki Yanagita[1,*], Kaishan Feng[1], Yuko Miyamura[1,2], Adi Azriff Basri[3], Mohammad Zuber[4], Siti Rohani[5], Abdul Aziz[6], Kamarul Arifin Ahmad[3], Masaaki Tamagawa[1]

[1] Graduate School of Life Science System and Engineering, Kyushu Institute of Technology, Fukuoka, Japan
[2] Department of Nursing, Faculty of Fukuoka Medical Technology, Teikyo University, Fukuoka, Japan
[3] Universiti Putra Malaysia, Malaysia
[4] Manipal Academy of Higher Education, India
[5] Hospital Kuala Lumpur, Malaysia
[6] Hospital Gleneagles, Malaysia

ARTICLE INFO

Article history:
Received 10 March 2023
Received in revised form 12 April 2023
Accepted 15 May 2023
Available online 30 June 2023

Keywords:
Airway; Virus Concentration; Risk Evaluation; CFD

ABSTRACT

Currently, Covid-19 is an epidemic all over the world. When virus directly adhere to mucous membrane of airway by breath, some humans maybe get inflammatory responses by viruses in the first stage of infection. The airway is composed of the nasal cavity, sinuses (Maxillary Sinus, Ethmoid Sinus, Frontal Sinus and Sphenoidal Sinus) and lungs. In the infection stage, the sinuses located in the nasal cavity tend to exhibit particularly high virus concentrations. Therefore, it is important to evaluate quantitatively the areas where viruses are likely to be adhered in the nasal cavity including sinuses. In this study, by CFD including concentration analysis the areas where viruses are likely to be adhered in the nasal cavity are predicted. As for the methods, the nasal cavity was made from 2D-CT image data by Itk-SNAP. For this computation in the nasal cavity continuity equation, Navier-Stokes equation and transport equation are used. And the transport of concentration was computed in the divided 4 parts of nasal cavity. As a result, it was found that the ratio of the concentration to the initial concentration in Ethmoid Sinus is approximately 0.6. It was found that Ethmoid Sinus is the areas where viruses are likely to be adhered and the areas can be predicted by computing the concentration.

1. Introduction

COVID-19 has mutated into various subspecies and has been taking many lives for a long time. Generally, the viruses are floating in the air by sneezing and talking, and the people are infected by inhaling them. When the viruses directly adhere to the mucous membrane of the airway by breath, some people may get inflammatory responses by viruses in the first stage of infection [1,2]. Recently, some studies have predicted the amount of minute particle that adhere to the nasal cavity [3-5]. But most researches have not included sinuses. Since the sinuses are tended to be that residence time in the sinuses is higher than other airway, it is important for quantitatively evaluating the adhesion areas of the viruses to consider the sinuses [6].

* *Corresponding author.*
E-mail address: yoshiki.yanagita267@mail.kyutech.jp (Yoshiki Yanagita)

https://doi.org/10.37934/arnht.13.1.96105

Although the flow of the nasal cavity has been known to be that a flow field in which turbulent and laminar flows mix, previous studies have shown that it is possible to predict the flow field in the nasal cavity using Computational Fluid Dynamics (CFD) [7-12]. According to Inthavong *et al.,* [7], flow patterns in the nasal cavity were investigated by CFD. It was found that the surrounding air flow to the other angle by the difference of the geometry. Besides, according to Yu *et al.,* [8], it was clarified that the maxillary sinus effects on the concentration in the nasal cavity through the concentration of the nitric oxide in the nasal cavity including the maxillary sinus is analyzed by CFD. However, the sinuses other than the maxillary sinus were not done modeling, and the effect of these sinuses on the velocity and the concentration in the nasal cavity is not shown.

In this study, the velocity, the pressure, and the concentration in the nasal cavity made from 2D CT image data were computed by CFD, and it is compared concentration in the nasal cavity divided into 4 parts (Maxillary Sinus, Ethmoid Sinus, Frontal Sinus and Sphenoidal Sinus).

2. Methodology

2.1 Obtainment and Smoothing of 3D Geometry of Nasal Cavity

The 3D geometry of the nasal cavity is obtained from 2D-CT image data by Itk-SNAP [13]. The medical image used to the obtained geometry of the nasal cavity was used the sample dataset of Pydicom. Therefore, the contrast is adjusted to be emphasized only the nasal cavity. Figure 1 shows the obtained geometry of nasal cavity from 2D-CT image data.

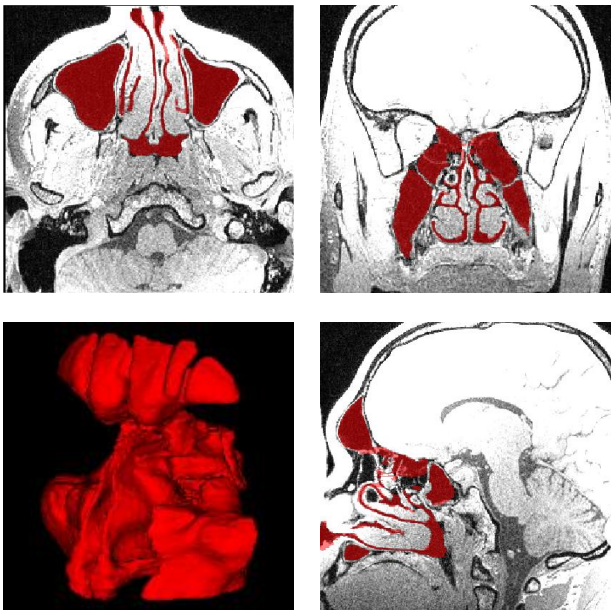

Fig. 1. Obtained geometry of nasal cavity from 2D-CT image data

To remove the noise from the obtained geometry due to the resolution of 2D-CT image data, the obtained geometry is smoothed by VMTK. The cut-off frequency of low pass filter for smoothing the geometry is setup, and the surface geometry can be smoothed by repeatedly processing. Generally, the surface geometry becomes smooth when the number of iterations for smoothing is higher. However, it is possible that the original geometrical properties are loss by setting the cut-off frequency and number of iterations of the low-pass filter if these parameters are not properly adjusted. In this case, the cut-off frequency of the low-pass filter is 0.1Hz, and the number of iterations is 30.

Figure 2 shows the location of the nasal cavity and the geometry of nasal cavity after smoothing. Figure 2(a) shows the location of the nasal cavity, and Figure 2(b) shows the geometry of nasal cavity after smoothing. Generally, the nasal cavity has four sinuses, and each region is defined: Region 1 is Maxillary Sinus, Region 2 is Ethmoid Sinus, Region 3 is Frontal Sinus, Region 4 is Sphenoidal Sinus (Figure 2(b)).

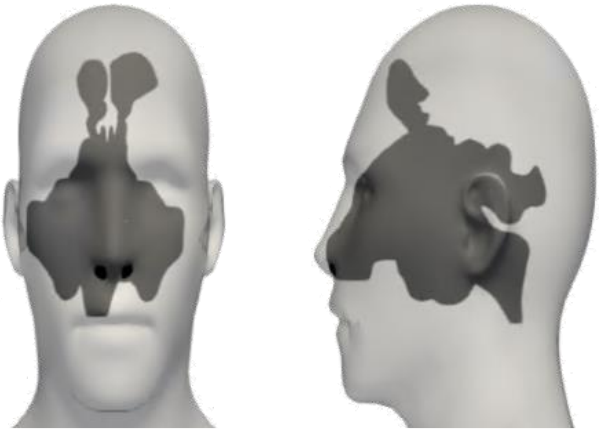

(a)

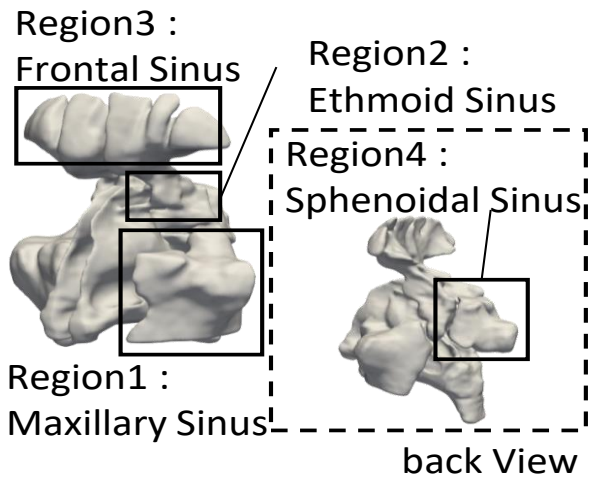

(b)

Fig. 2. Objective model (a) Location of the nasal cavity (b) Geometry of nasal cavity after smoothing

2.2 Computational Method
2.2.1 Governing equations

As the flow is assumed to be incompressible, steady and turbulent flow, continuity equation and Navier-Stokes equation are used [4,5]. These equation shows following:

$$\nabla \cdot \bar{u} = 0 \tag{1}$$

$$\frac{\partial \bar{u}}{\partial t} + \nabla \cdot (\bar{u}\bar{u}) = -\frac{1}{\rho}\nabla \bar{p} + (\nu + \nu_t)\,\nabla^2 \bar{u} \tag{2}$$

where ρ is density, $\bar{\boldsymbol{u}}$ is averaged velocity, $\bar{p}$ is averaged pressure, ν is kinematic viscosity, ν_t is coefficient of turbulence (= $C\mu\rho k^2/\varepsilon$).

The turbulent model is *k* - *ε* model, and the coefficient of turbulence is calculated by solving the following two transport equations [6]:

$$\frac{\partial k}{\partial t} + \bar{u}\nabla k = -\bar{u}\bar{u}\nabla\bar{u} + \nabla\left\{\left(\frac{\nu_t}{\sigma_k} + \nu\right)\nabla k\right\} \tag{3}$$

$$\frac{\partial \varepsilon}{\partial t} + \bar{u}\nabla\varepsilon = (-C_{\varepsilon 1}\bar{u}\bar{u}\nabla\bar{u} - C_{\varepsilon 2}\varepsilon)\frac{\varepsilon}{k} + \nabla\left\{\left(\frac{\nu_t}{\sigma_\varepsilon} + \nu\right)\nabla\varepsilon\right\} \tag{4}$$

where $C\mu$ (= 0.09), σ_k (= 1.0), $C_{\varepsilon 1}$ (= 1.44), $C_{\varepsilon 2}$ (= 1.92), σ_ε (= 1.3) is model coefficient. The coefficient of turbulence ν_t is calculated after *k* and *ε* are obtained by solving Eq. (3) and Eq. (4). The flow fields can be solved by assigning the calculated coefficient of turbulence to Eq. (1) and Eq. (2). The virus concentration is calculated by solving the following transport equation [4,14]:

$$\frac{\partial c}{\partial t} + \nabla\cdot(\bar{u}c) - (D_m + D_t)\nabla^2 c = S_C \tag{5}$$

where c is virus concentration, D_m is molecular diffusion coefficient (= $\sqrt{8k_bT/\{\pi m\}}/\{3\sqrt{2}\pi n d^2\}$), k_b is Boltzmann constant, T is Temperature, m is molecular mass, n is molecular density, D_t is turbulence diffusion coefficient (= ν_t/Sc_t), Sc_t is turbulence Schmidt number (= 1), S_C is source term. In this case, the turbulent Schmidt number set to be 1, and it is assumed concentration and velocity boundary layers are the same. Besides, virus aerosol diameter is assumed to be 1 μm, and the diffusion coefficient was calculated based on the mass of the COVID-19 virus obtained from measurements [15,16].

The areas where the virus tends to stay are evaluated by the residence time. The residence time is calculated by the following equation:

$$\nabla\cdot(\rho\bar{u}\tau) = 1 \tag{6}$$

The residence time can show time that takes for a particle to travel from the entrance to its location.

2.2.2 Boundary conditions

Figure 3 shows the analysis model, and Table1 shows the boundary conditions. Air flow passes the nostrils into the pharynx. The initial condition is set that the concentration in the analysis area is distributed at a constant level (c_0 = 4.98×10^{-12} mol/m^3). Inlet boundary condition is set up to be that the pressure is atmospheric pressure (p = 0 Pa), and the concentration source is the same initial concentration. Outlet boundary condition is set up to be that the distribution is fully developed velocity based on the averaged velocity. In this case, since continuity equation can be maintained and the calculation stabilized by the air to flow out, outlet boundary condition is set up velocity condition. The non-slip boundary condition was set for the wall.

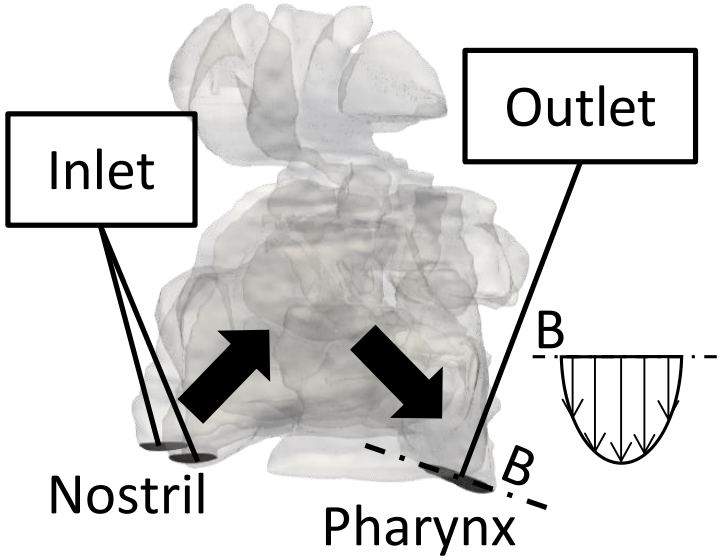

Fig. 3. Analysis model

Table 1
Boundary conditions

	p [Pa]	u (x, y, z) [m/s]	c [mol/m^3]
Initial Condition	$p = 0$	$u = 0$	$c = 4.98\times10^{-12}$
Inlet Boundary Condition	$p = 0$	$\partial u/\partial n = 0$	$c = 4.98\times10^{-12}$
Outlet Boundary Condition	$\partial p/\partial n = 0$	$u_n=2Q_m/A$	$\partial c/\partial n = 0$
		$Q_m = 5.83\times10^{-4}$ [m^3/s]	
Wall Boundary Condition	$\partial p/\partial n = 0$	$u = 0$	$c = 0$

3. Results and Discussions

3.1 Acquisition Positions of Distribution

In the results and the discussion, the velocity and the concentration distribution are obtained on reference plane. Figure 4 shows the reference plane to obtain the velocity, the residence time, and the concentration distribution.

3.2 Velocity Distribution

To find the region that the velocity is large, the velocity distribution is considered. Figure 5 shows the velocity distribution on the reference plane (Figure 4). It is shown that the velocity is large in the main part of the nasal cavity, but the velocity in the sinuses is small. In other words, airflow exchange into the sinuses can be seen that is small.

Figure 6 shows the path line. The locations of the tracking particles to generate path line are the downstream side and the upper nasal cavity. It can be seen that the velocity increases in the nostrils and pharynx. Besides, vortices are generated in these areas. According to the velocity distribution (Figure 5) and the path line (Figure 6), most of the airflow flows into the pharynx without flowing into the sinuses.

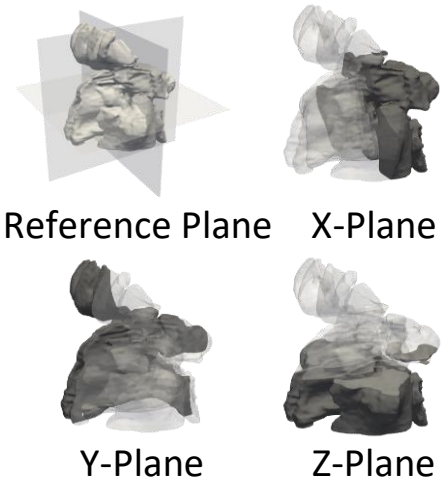

Fig. 4. Reference plane for obtained the velocity, the residence time, and the concentration distribution

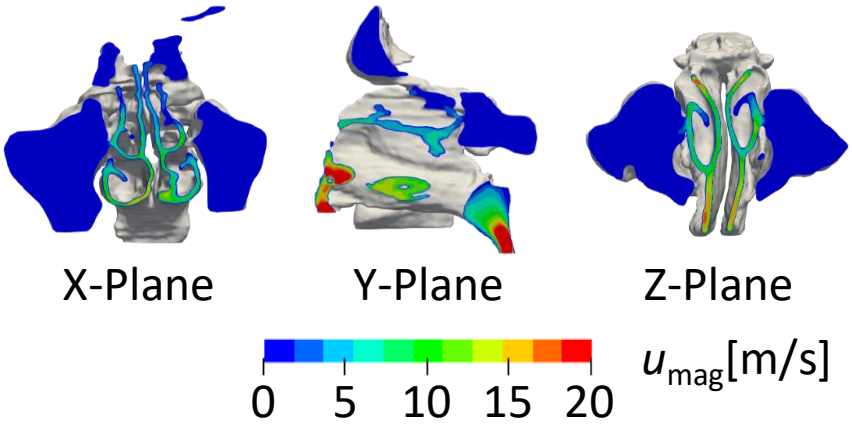

Fig. 5. Velocity distribution on the reference plane

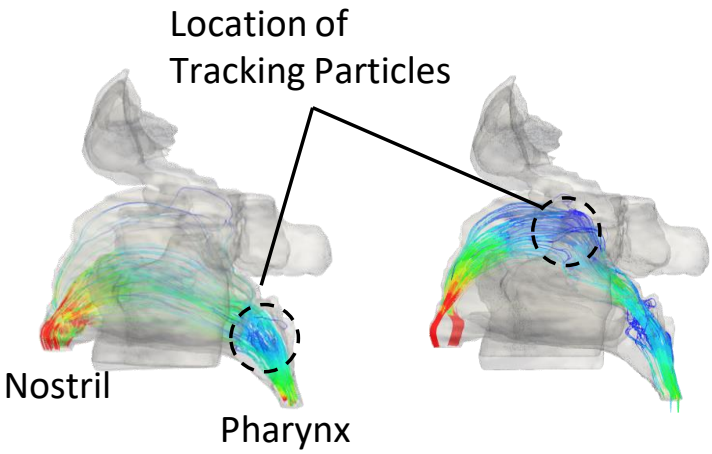

Fig. 6. Path line

3.3 Concentration Distribution

Virus concentrations were calculated by solving Eq. (5). Since the initial concentration (c_0 = 4.98×10^{-12} mol/m^3) is filled in the analysis area, the virus concentration is divided by the initial

concentration to evaluate the dimensionless value. Figure 7 shows the concentration distribution on the reference plane (Figure 4). It can be seen that the residence time decreases in the mainstream of the nasal cavity and nostrils and the pharynx but increases in the sinuses such as Maxillary Sinus. It was found that the possibility of the virus adhesion is high in the nostrils and pharynx. Especially, since the concentration in the pharynx is high and tends to be stagnant airflow, it is suggested that it is the most likely area of adhesion within the nasal cavity.

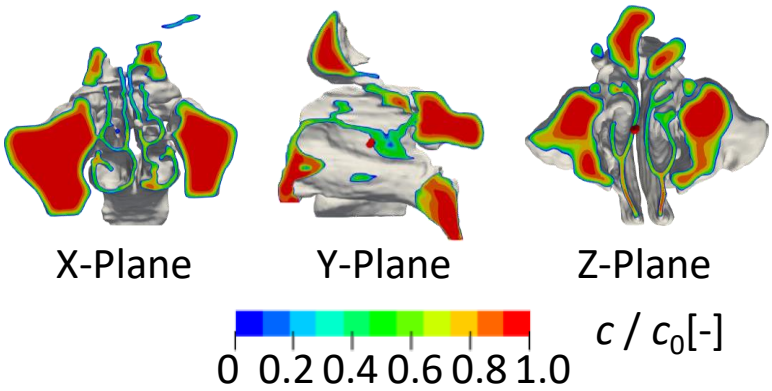

Fig. 7. Concentration distribution on the reference plane

Figure 8 shows the residence time distribution on the reference plane (Figure 4). It can be seen that the residence time is longer in all sinuses. It is suggested that the virus is high to stay in these regions. Therefore, the region where the possibility of the virus adhesion is high other than the mainstream is investigated. In order to quantitatively compare the concentration in the sinus, nasal cavity divided into four regions and the concentration in the sinus is quantitatively calculated based on the volume-averaged concentration. Figure 9 shows divided the nasal cavity into four regions. The definition of volume-averaged concentration shows following equation:

$$(c/c_0)_{ave} = \frac{1}{V}\int c/c_0 dV \tag{7}$$

where V is volume in each region. Figure 10 shows the comparison of volume-averaged concentration in each region. It can be seen that the volume-averaged concentration is the largest in Region 1 and the smallest in Region 2.

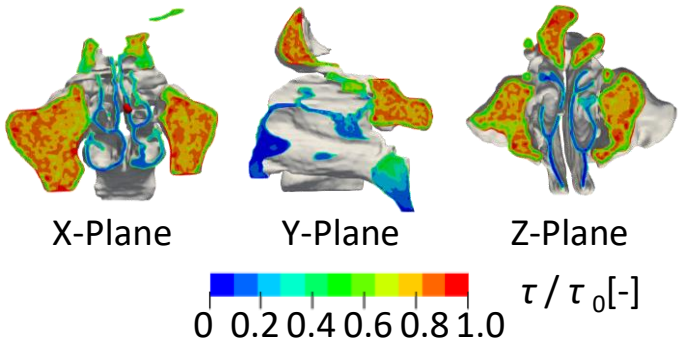

Fig. 8. Residence time distribution on the reference plane

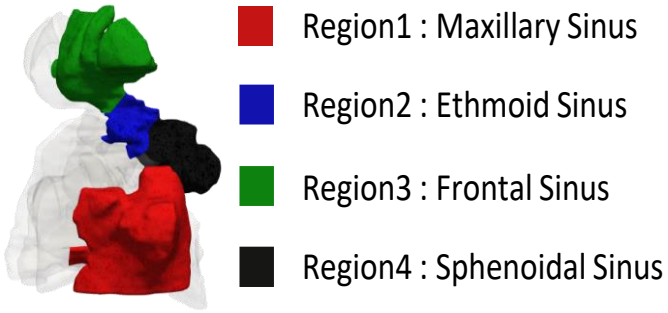

Fig. 9. Concentration distribution on the reference plane

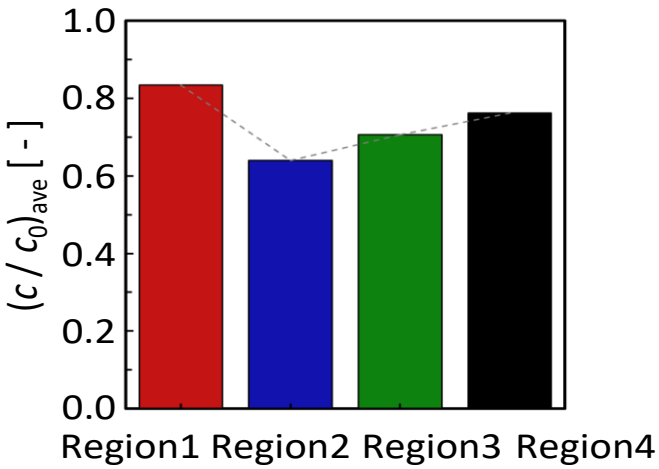

Fig. 10. Comparison of volume-averaged concentration in each region

However, according to the velocity distribution (Figure 5), the velocity in the Region 1 is small. In other words, it is predicted that the virus is unlikely to adhere to the area because the possibility of air into Region 1 is small. Therefore, the following equation is defined to consider the effect of the initial concentration:

$$\begin{cases} j = 1 & |u - u_0| > \sqrt{D_m/T} \\ j = 0 & |u - u_0| \leq \sqrt{D_m/T} \end{cases}$$

$$(c/c_0)_J = j(c/c_0) \tag{8}$$

$$(c/c_0)_{ave,J} = \frac{1}{V}\int (c/c_0)_J dV \tag{9}$$

The equation discerns the velocity change due to molecular diffusion, and the volume-average concentrations were evaluated only in the region that the change of velocity is larger than molecular diffusion. Figure 11 shows the concentration distribution using Eq. (9). By using the equation, the effect of the initial concentration can be considered, and the concentration in the Region 1 (Maxillary Sinus) is small. Figure 12 shows the comparison of volume-averaged concentration using Eq. (9) in each region. It can be seen that the influence of the initial concentration is large the concentration in Regions 1 and 3. On the other hand, Region 2 has the highest concentration because the air flows into Region 2 and the concentration stays. Therefore, it is suggested that Region 2 is the area where the virus is most likely to be adhered.

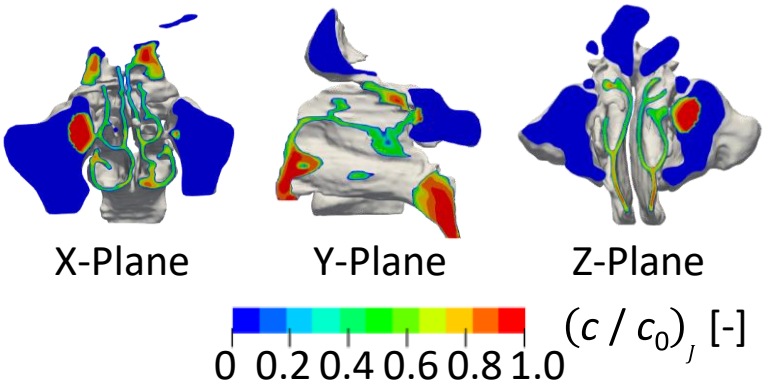

Fig. 11. Concentration distribution on the reference plane

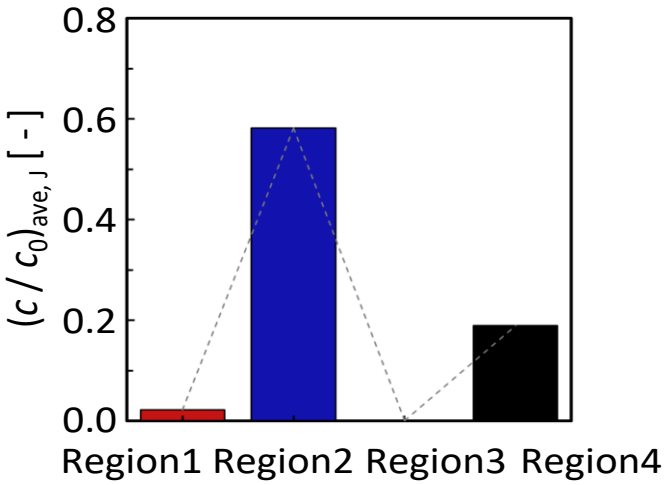

Fig. 12. Comparison of volume-averaged concentration using Eq. (9) in each region plane

4. Conclusion

In our paper, it is found that the concentration in the pharynx is high and tends to be stagnant airflow. As the result, it is suggested that it is the most likely area of adhesion within the nasal cavity. In addition, it is suggested that Region 2 (Ethmoid Sinus) is the area where the virus is most likely to adhere.

Acknowledgement

A part of this research was supported by the Co-Funding Research Program by and between Kyushu Institute of Technology (KYUTECH) and Universiti Putra Malaysia (UPM).

References

[1] Zhu, Na, Dingyu Zhang, Wenling Wang, Xingwang Li, Bo Yang, Jingdong Song, Xiang Zhao et al. "A novel coronavirus from patients with pneumonia in China, 2019." *New England journal of medicine* 382, no. 8 (2020): 727-733. https://doi.org/10.1056/NEJMoa2001017

[2] Wang, Chen, Peter W. Horby, Frederick G. Hayden, and George F. Gao. "A novel coronavirus outbreak of global health concern." *The lancet* 395, no. 10223 (2020): 470-473. https://doi.org/10.1016/S0140-6736(20)30185-9

[3] Zuber, Mohammad, John Valerian Corda, Milad Ahmadi, B. Satish Shenoy, Irfan Anjum Badruddin, Ali E. Anqi, Kamarul Arifin Ahmad et al. "Investigation of coronavirus deposition in realistic human nasal cavity and impact of social distancing to contain COVID-19: A computational fluid dynamic approach." *Computer Modeling in Engineering & Sciences* 125, no. 3 (2020): 1185-1199. https://doi.org/10.32604/cmes.2020.015015

[4] Schroeter, Jeffry D., Julia S. Kimbell, Bahman Asgharian, Earl W. Tewksbury, and Madhuri Singal. "Computational fluid dynamics simulations of submicrometer and micrometer particle deposition in the nasal passages of a Sprague-Dawley rat." *Journal of aerosol science* 43, no. 1 (2012): 31-44. https://doi.org/10.1016/j.jaerosci.2011.08.008

[5] Li, Xiangdong, Kiao Inthavong, and Jiyuan Tu. "Particle inhalation and deposition in a human nasal cavity from the external surrounding environment." *Building and Environment* 47 (2012): 32-39. https://doi.org/10.1016/j.buildenv.2011.04.032

[6] Mortazavi, Hamed, Hamidreza Mortazavy Beni, Fatemeh Aghaei, and Seyed Hossein Sajadian. "SARS-CoV-2 droplet deposition path and its effects on the human upper airway in the oral inhalation." *Computer Methods and Programs in Biomedicine* 200 (2021): 105843. https://doi.org/10.1016/j.cmpb.2020.105843

[7] Inthavong, Kiao, Jiawei Ma, Yidan Shang, Jingliang Dong, Annicka SR Chetty, Jiyuan Tu, and Dennis Frank-Ito. "Geometry and airflow dynamics analysis in the nasal cavity during inhalation." *Clinical Biomechanics* 66 (2019): 97-106. https://doi.org/10.1016/j.clinbiomech.2017.10.006

[8] Yu, Shen, Danqing Wang, Yan Guo, Shuang Shen, and Jizhe Wang. "Numerical study on the distribution of nitric oxide concentration in the nasal cavity of healthy people during breathing." *Nitric Oxide* 130 (2023): 12-21. https://doi.org/10.1016/j.niox.2022.11.002

[9] Corda, John Valerian, B. Satish Shenoy, Leslie Lewis, S. M. Khader, Kamarul Arifin Ahmad, and Mohammad Zuber. "Nasal airflow patterns in a patient with septal deviation and comparison with a healthy nasal cavity using computational fluid dynamics." *Frontiers in Mechanical Engineering* 8 (2022): 1009640. https://doi.org/10.3389/fmech.2022.1009640

[10] Wedel, Jana, Paul Steinmann, Mitja Štrakl, Matjaž Hriberšek, and Jure Ravnik. "Can CFD establish a connection to a milder COVID-19 disease in younger people? Aerosol deposition in lungs of different age groups based on Lagrangian particle tracking in turbulent flow." *Computational Mechanics* 67 (2021): 1497-1513. https://doi.org/10.1007/s00466-021-01988-5

[11] Basu, Saikat. "Computational characterization of inhaled droplet transport to the nasopharynx." *Scientific Reports* 11, no. 1 (2021): 6652. https://doi.org/10.1038/s41598-021-85765-7

[12] Brüning, Jan, Thomas Hildebrandt, Werner Heppt, Nora Schmidt, Hans Lamecker, Angelika Szengel, Natalja Amiridze et al. "Characterization of the airflow within an average geometry of the healthy human nasal cavity." *Scientific reports* 10, no. 1 (2020): 3755. https://doi.org/10.1038/s41598-020-60755-3

[13] Yushkevich, Paul A., Joseph Piven, Heather Cody Hazlett, Rachel Gimpel Smith, Sean Ho, James C. Gee, and Guido Gerig. "User-guided 3D active contour segmentation of anatomical structures: significantly improved efficiency and reliability." *Neuroimage* 31, no. 3 (2006): 1116-1128. https://doi.org/10.1016/j.neuroimage.2006.01.015

[14] Corley, Richard A., Senthil Kabilan, Andrew P. Kuprat, James P. Carson, Kevin R. Minard, Richard E. Jacob, Charles Timchalk et al. "Comparative computational modeling of airflows and vapor dosimetry in the respiratory tracts of rat, monkey, and human." *Toxicological Sciences* 128, no. 2 (2012): 500-516. https://doi.org/10.1093/toxsci/kfs168

[15] Qu, Guangbo, Xiangdong Li, Ligang Hu, and Guibin Jiang. "An imperative need for research on the role of environmental factors in transmission of novel coronavirus (COVID-19)." (2020): 3730-3732. https://doi.org/10.4164/sptj.57.526

[16] White, Nathan, John-David Seelig, and Sudarshan K. Loyalka. "Computation of drag and diffusion coefficient for coronavirus: I." *Journal of Aerosol Science* 157 (2021): 105806. https://doi.org/10.1016/j.jaerosci.2021.105806